THE JOURNAL OF PHYSICAL CHEMISTRY Letters

Letter

pubs.acs.org/JPCL

Dynamic Determination of Active-Site Reactivity in Semiquinone Photolyase by the Cofactor Photoreduction

Zheyun Liu, Chuang Tan, Xunmin Guo, Jiang Li, Lijuan Wang, and Dongping Zhong*

Department of Physics, Department of Chemistry and Biochemistry, and Programs of Biophysics, Chemical Physics, and Biochemistry, The Ohio State University, Columbus, Ohio 43210, United States

Supporting Information

ABSTRACT: Photolyase contains a flavin cofactor in a fully reduced form as its functional state to repair ultraviolet-damaged DNA upon blue light absorption. However, after purification, the cofactor exists in its oxidized or neutral semiquinone state. Such oxidization eliminates the repair function, but it can be reverted by photoreduction, a photoinduced process with a series of electron-transfer (ET) reactions. With femtosecond absorption spectroscopy and site-directed mutagenesis, we completely recharacterized such photoreduction dynamics in the semiquinone state. Comparing with all previous studies, we identified a new intramolecular ET pathway, determined stretched ET behaviors, refined all ET time scales, and finally evaluated the driving forces and reorganization energies for eight elementary ET reactions. Combined with the oxidized-state photoreduction dynamics, we elucidated the different active-site properties of the reduction ability and structural flexibility in the oxidized and semiquinone states, leading to the dramatically different ET dynamics and photoreduction efficiency in the two states.

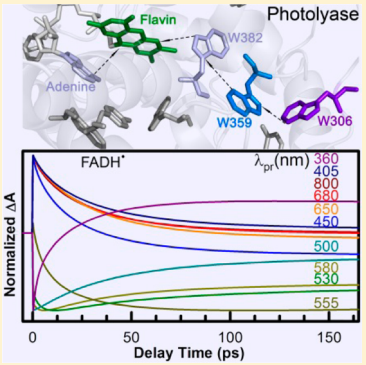

SECTION: Biophysical Chemistry and Biomolecules

The ultraviolet (UV)-induced photolesions in DNA can cause its mutagenesis and even lead to skin cancer.[1] Such damaged DNA can be repaired by a class of photoenzyme, photolyase, upon blue light perception.[2−5] All photolyases noncovalently bind with a flavin adenine dinucleotide as the catalytic cofactor. The functional state of the catalytic cofactor in photolyase is an anionic hydroquinone ($FADH^-$) in vivo[5,6] that has been determined recently as an only feasible active state.[7] However, the flavin cofactor after purification becomes to a neutral semiquinone ($FADH^•$) or fully oxidized (FAD) state. These two states in vitro can be easily reduced through a photoinduced electron-transfer (ET) process (namely, photoreduction).[8,9] The dynamics of such photoreduction of $FADH^•$ has been reported extensively with femtosecond (fs) resolution.[9−16] In those studies, a nearby tryptophan was reported to donate one electron to the $FADH^•$ cofactor in 45 ps,[9,13] and the subsequent electron hopping occurs within a conserved tryptophan triad system (W382, W359, and W306 in Figure 1)[14,17] within 30 ps, competing with charge recombination steps.[13] The surface-exposed W306 in the triad is the most critical residue because the $W306^+$ radical deprotonates or accepts one electron from solution so that the reduced cofactor can be stabilized for a long time.[9,14] In the X-ray structure,[17] there are several potential electron donors (tryptophan, tyrosine, and the adenine moiety) surrounding the flavin cofactor (Figure 1), and thus, the flavin cofactor could be reduced through multiple pathways. We have recently reported the complete characterization of oxidized-state photoreduction of FAD in photolyase and revealed that with the conserved tryptophan triad, two additional tryptophan residues (W384 and W316 in Figure 1) and the adenine moiety of the cofactor constitute three layers of electron donors and thus reduce the

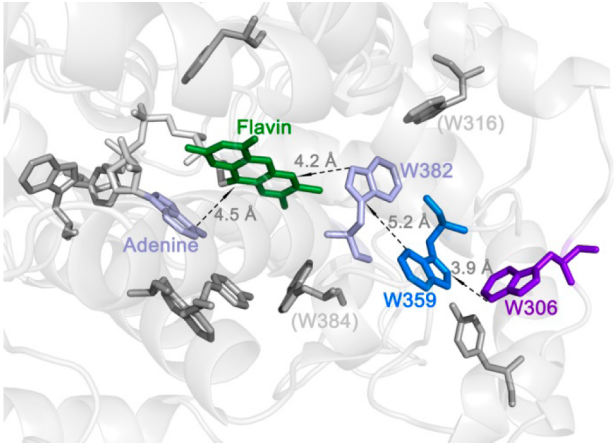

Figure 1. The X-ray structure around the active site with ET networks for photoreduction in semiquinone photolyase with all tunneling distances shown. The flavin moiety (green) of the cofactor behaves as an electron sink to draw electron flow from a series of aromatic molecules. The adenine moiety and W382 (light blue) have direct ET with the flavin moiety, while the W359 (dark blue) and W306 (purple) residues follow a consecutive electron tunneling to the protein surface. All other aromatic residues are not involved in photoreduction.

Received: January 12, 2014
Accepted: February 11, 2014
Published: February 11, 2014

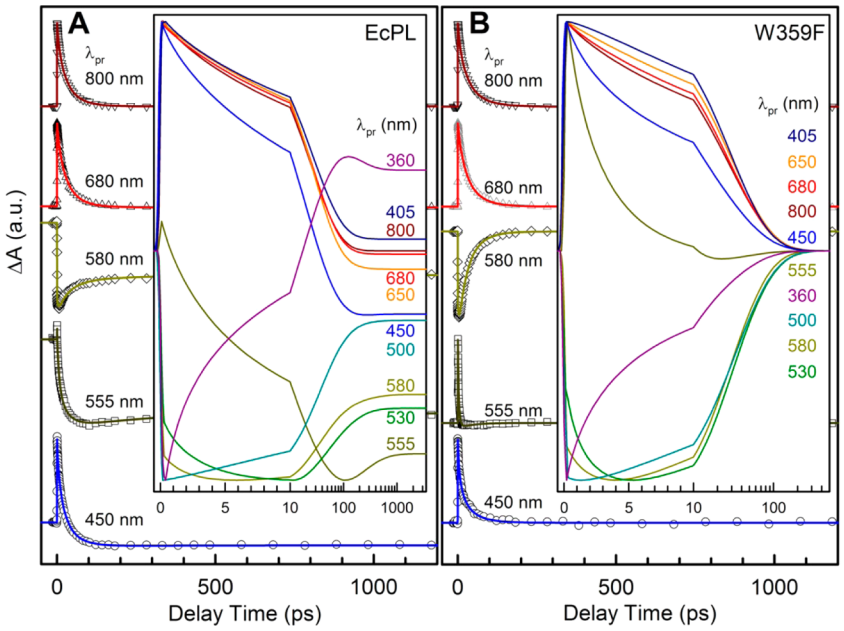

Figure 2. Femtosecond-resolved absorption transients of photoreduction (A) EcPL (E109A mutant) and (B) W359F. The ET dynamics are probed systematically from 800 to 360 nm, and shown are several typical transients with a distinct pattern. Insets show the fitting curves probed at 10 different probe wavelengths, and the results are plotted by a linear scale before 10 ps and by a logarithmic scale after 10 ps.

oxidized cofactor with a high efficiency through a reduction gradient.[18] With the finding of new electron donors, we extend here to recharacterize the photoreduction of $FADH^{\bullet}$ by mapping out the complete electron flow dynamics. The obtained results can be directly compared with the previous studies on the oxidized state,[18] more importantly, to reveal the critical differences in the ET dynamics at the active site due to the two different redox states.

Using an E109A mutant photolyase as the template (EcPL) to eliminate the second chromophore (MTHF)[19] for experimental simplicity, we prepared four tryptophan mutants (W382F/W384F, W382F, W359F, and W306F in Figure 1) to differentially block the possible electron tunneling pathway(s). We systematically studied the photoreduction dynamics of various ET processes for the four mutant and wild-type proteins with excitation at 620 or 640 nm. Figure 2 shows the typical transients of the wild-type and W359F mutant with a series of probing wavelengths from 800 to 360 nm to detect the dynamics of initial reactants, subsequent intermediates, and final products. The experimental details, three other mutant transients (Figures S1−S3), and data analyses are all given in the Supporting Information (SI). Clearly, Figure 2 shows a series of features for different probing wavelengths, reflecting the detection of various species. For the three mutants (W282F/W384F, W382F, and W359F), all signals decay to zero in our time window of 3 ns (Figures 2B and S1 and S2 (SI)), indicating that the reactions are complete and all species return to the original ground states. For the wild-type and W306F (Figures 2A and S3 (SI)), the transients decay on a much longer time scale, manifesting the relatively long-lived species of W^{+} and $FADH^{-}$. For W306F, the signals finally decay to zero, and the $FADH^{\bullet}$ cannot be successfully reduced, while for the wild-type, the surface-exposed $W306^{+}$ may obtain one electron from bulk solution and the $FADH^{\bullet}$ can be permanently reduced to $FADH^{-}$, finishing the photoreduction process.

Specifically, with W382F/W384F, we eliminated the neighboring tryptophan residues as possible electron donors (Figure 1), and the only electron donor is the adenine moiety of the cofactor.[7,18] Interestingly, the double mutant shows nearly identical dynamics as the W382F mutant (Figures S1 and S2, SI), indicating that the ET from W384 is extremely slow compared with that for the competing adenine channel, and thus, the involvement of W384 in photoreduction is negligible. Similar to the oxidized cofactor,[18] we observed that the excited state of the neutral semiquinoid lumiflavin (the isoalloxazine ring) moiety ($LfH^{\bullet}$*) follows a stretched exponential decay ($I = Ae^{-(t/\tau)^{\beta}}$) with a time constant of τ = 82 ps and a stretched parameter β = 0.93, leading to an averaging reaction time ($\langle\tau\rangle = (\tau/\beta)\Gamma(1/\beta)$) of 85 ps. The stretched behavior results from the coupling of the ET dynamics with the local protein relaxation. The active-site solvation in the fully reduced $FADH^{-}$ state has been measured on a wide time scale from a few picoseconds to subnanoseconds,[20] and similar relaxation time scales are expected in the semiquinone $FADH^{\bullet}$ state.[21] In the previous studies,[9−13] the dynamics were fitted to follow a single-exponential decay, and the dynamics observed in W382F was attributed to the intrinsic lifetime of $FADH^{\bullet}$*.[10] However, considering that the lifetime of $LfH^{\bullet}$* in a semiquinone flavodoxin,[22] 230 ps, is obviously longer than 85 ps and the intramolecular ET reaction from the adenine to lumiflavin moieties in the cofactor flavin has a favorable free energy (−0.03 eV),[7] the observed 85 ps component is indeed from both contributions of the lifetime emission ($\tau_l \approx 230$ ps; see Figure 3A) and charge separation in 135 ps ($\langle\tau_{FAde}\rangle$). In the X-ray structure,[17] the lumiflavin and adenine moieties are in close contact, and thus, the active-site solvation process minimally influences the intramolecular ET process between the two moieties, leading to a stretched parameter of 0.93 that is close to 1.[7] To confirm the intramolecular ET, we further extended the probing wavelengths and obtained the intermediate signal of the adenine cation (Ade^{+}) (Figure S1, SI). By the systematic fitting of the

dx.doi.org/10.1021/jz500077s | J. Phys. Chem. Lett. 2014, 5, 820−825

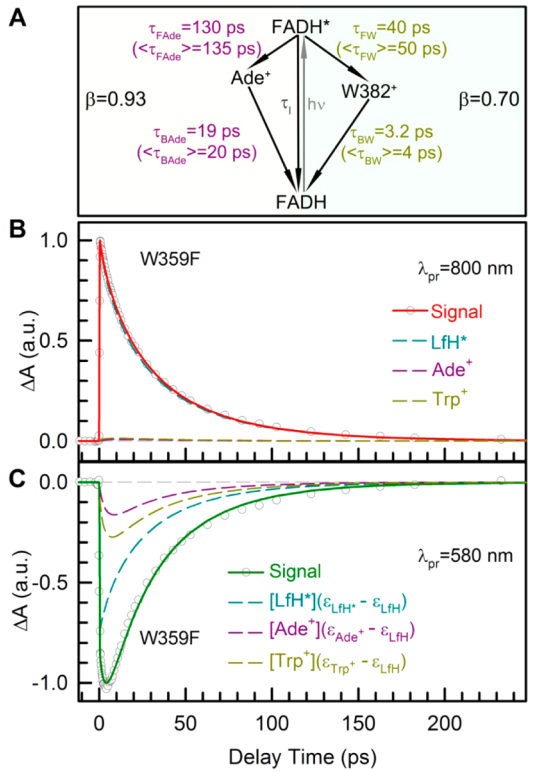

Figure 3. Dynamics and mechanism of ET reactions in W359F mutant. (A) The two obtained ET channels involving the adenine moiety and W382. The left light-yellow panel shows the ET dynamics between the isoalloxazine ring and the adenine moiety with a stretching constant of 0.93, and the right light-green panel summarizes the ET dynamics between the isoalloxazine ring and W382 with a more stretched constant of 0.70. (B,C) Normalized transient absorption signals of W359F mutant probed at 800 and 580 nm with the decomposed dynamics of the initial reactant, various intermediates, and final product.

transients at 10 different probing wavelengths, the charge recombination was found to occur within 20 ps ($\langle\tau_{BAde}\rangle$ in Figure 3A). Such slower charge separation and faster charge recombination lead to less accumulation of the intermediates and, in fact, prevent the photoreduction of FADH•.

Knowing the intramolecular ET, we further studied the dynamics of W359F mutant, which includes W382 into the ET network (Figures 2B and 3). At 800 nm, we also mainly probed the signals of LfH•* that now follows three parallel decay pathways, the lifetime emission (τ_l), intramolecular ET with the adenine moiety (τ_{FAde}), and intermolecular ET with W382 residue (τ_{FW}); see Figure 3A and B. We solved the charge separation between W382 and the LfH• moiety in 40 ps with a stretched parameter β = 0.70 (see the data analyses in the SI), leading to an averaged ET time $\langle\tau_{FW}\rangle$ = 50 ps. The stretched parameter β = 0.70 is much smaller than that of the same ET pair at the oxidized state (τ = 0.8 ps and β = 0.92),[18] indicating that the dynamics is more stretched, consistent with the longer ET time that is strongly coupled with the local protein relaxation. Tuning the probing wavelengths to the blue side, we detected the intermediates of Ade^+ and $W382^+$, and Figure 3C shows the transient probed at 580 nm. The signal can be regrouped into three categories; the first component is from the dynamics of the excited state, the second one represents the dynamics of Ade^+, and the third component reflects the dynamics of the $W382^+$ intermediate. Because the ground-state LfH• has a larger absorption coefficient than those of all other species,[7,23,24] the transient signal flips, and all components show negative. Knowing the dynamics of various previous steps and after the systematic analyses of more than 10 transients, the charge recombination between $W382^+$ and LfH^- was determined to occur in 4 ps ($\langle\tau_{BW}\rangle$ in Figure 3A). With W382F and W359F mutants, we did not observe any noticeable electron tunneling between $W382^+$ and W316. Thus, this ET step should be much slower than the charge combination in 4 ps.

Similarly, we analyzed the transients of W306F (Figure S3, SI) and the wild-type (Figure 2A) step by step (data analyses are given in the SI), and the dynamics and time scales are finally shown in Figure 4A. The W306F mutant shows a drastically

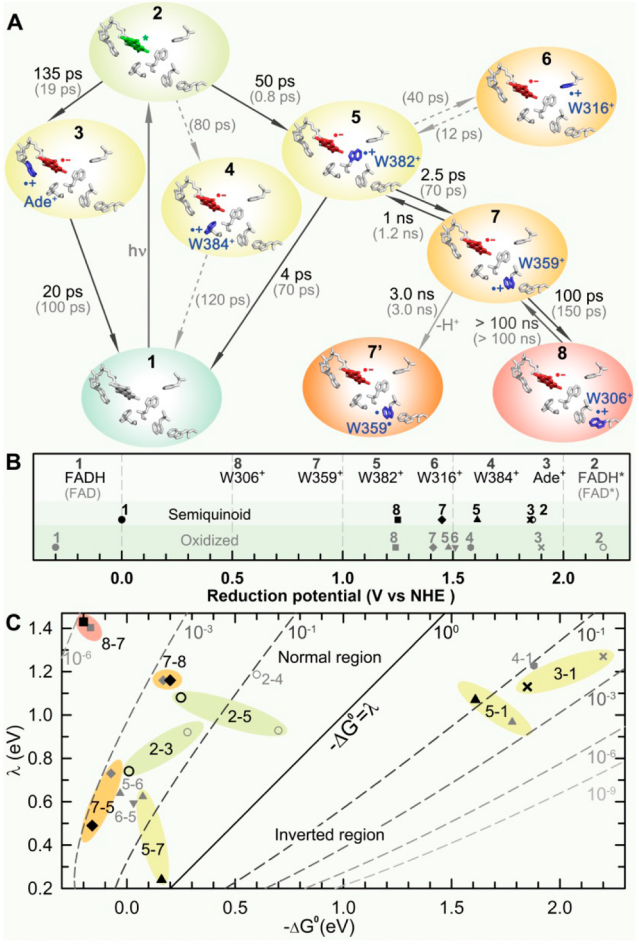

Figure 4. Comparison of photoreduction dynamics of the oxidized and semiquinoid photolyase with a series of ET reactions. (A) Dynamics and time scales of all elementary ET steps at the neutral semiquinoid state (black) and the oxidized state (gray). Note that some ET channels may not be active in the semiquinoid state. (B) The derived reduction potentials of all involved species (black for the semiquinone and gray for the oxidized). (C) Two-dimensional (2D) plot of the Franck−Condon (energy) parts of ET rates relative to free energy (ΔG^0) and reorganization energy (λ) for all electron tunneling steps with an electronic-coupling constant of β = 1.4 Å^{-1}. The charge recombination steps with the flavin moiety at both redox states fall in the Marcus inverted ET region ($-\Delta G^0 > \lambda$), and all other ET reactions fall in the Marcus normal region ($-\Delta G^0 \leq \lambda$). The highlighted ovals group the same ET processes in the two redox states for comparison of their driving forces and reorganization energies; see the text.

dx.doi.org/10.1021/jz500077s | J. Phys. Chem. Lett. 2014, 5, 820−825

different dynamic behavior from W359F. We found that the W359 donates an electron to $W382^+$ in 2.5 ps, much faster than that (70 ps) in oxidized photolyase. The resulting $W359^+$ either deprotonates to $W359^\bullet$ in 3 ns, similar to that observed in the oxidized state,[18] or proceeds to charge relocation to W382 in 1 ns. This back ET step is much slower than the forward ET (2.5 ps), providing a larger probability for $W359^+$ to stay for a long time and thus facilitating further electron tunneling from the outside electron donor W306. The final electron tunneling step between $W359^+$ and W306 in the wild-type (EcPL in Figure 2A) has similar dynamics and time scales of the faster forward ET in 100 ps and slower back ET in >100 ns as those observed in the oxidized state[18] (Figure 4A), further confirming the reduction potential gradient and thus resulting in successful photoreduction.

All of the dynamics and time scales of the cofactor photoreduction in the two states, oxidized and semiquinoid, are show in Figure 4A. Because the photoreduction of neutral semiquinoid $FADH^\bullet$ in photolyase has been extensively studied in the past decade,[9−16] it is necessary to summarize the difference between the current work and previous studies. Using the wild-type EcPL and four tryptophan mutants, in this work, we completely resolved the dynamics of electron flow toward the catalytic center of the neutral semiquinoid flavin cofactor within the ET network. First, we revealed a new initial ET channel of intramolecular charge separation between the lumiflavin and adenine moieties. This channel is significant and branches out 27% of the excite-state populations, leading to a futile ET redox cycle and explaining the less photoreduction efficiency than that in the oxidized state that only has 4% in the intramolecular ET channel.[18] Second, we have to fit all ET dynamics in a stretched-exponential behavior rather than a single-exponential decay used in early studies.[9−13] From the dynamic point of view, the stretched behavior makes perfect sense due to the strong coupling between the local protein relaxation and ET dynamics on the similar ps time scales. Such nonequilibrium ET dynamics could be treated by the 2D Sumi−Marcus ET model,[25] and the protein dynamics could modulate the ET dynamics,[26] leading to nonexponential behavior.[2−4,7,18,26−28] Moreover, the ET dynamics of the lumiflavin moiety with the adenine moiety and W382 show different stretched parameters, β = 0.93 and 0.70, respectively, due to their different local environments surrounding the ET donors. Third, all of the ET times are revised due to the new intramolecular channel and different dynamic models of the ET processes. Also, we observed a relatively slower ET between $W359^+$ and W306 in 100 ps, not 30 ps as reported before.[12] Finally, we fitted the back ET between $W359^+$ and LfH^- in a consecutive step from W382 to $W359^+$ (1 ns) and then from LfH^- to $W382^+$ (4 ps), not a single step from LfH^- directly to $W359^+$ in 1.2 ns as reported.[13] The distance from LfH^- to $W359^+$ is about 9.9 Å, and the ET must be slow. The intervening W382 would be an ideal electron shuttle in the middle of tunneling, as also reported in the other protein.[29]

With four ET pairs and eight ET times, we can estimate the driving forces for the eight elementary ET steps using the similar strategy as that in the oxidized photolayse.[18] We assume that the mutation of tryptophan by phenylalanine will not significantly alter the reduction potentials of the cofactor flavin and other nearby tryptophans. Using the rates of forward and back ET reactions between the nearby tryptophan triad, we first obtained the free-energy gradient (ΔG^0) as −160 and −200 meV for $W382^+$/W359 and $W359^+$/W306 pairs, respectively. If we assume that the distant W306 residue, ∼15 Å from the cofactor, is minimally influenced by the redox change of the cofactor, the reduction potentials of $W359^+$/W359 and $W382^+$/W382 are derived to be 1.45 and 1.61 V versus NHE, respectively, with a known $W306^+$/W306 potential of ∼1.25 V versus NHE as used in oxidized photolyase.[18] Considering that the transition energy of $S_1 \leftarrow S_0$ for the neutral semiquinoid state is about 1.86 eV (∼670 nm) and $FADH^\bullet$ in photolyase has a reduction potential of ∼0 V versus NHE,[30] the ET from W382 to $FADH^\bullet$ has a favorable driving force of −0.25 eV, and the corresponding back ET from $FADH^-$ to $W382^+$ is −1.61 eV. Similar to the oxidized photolyase,[18] the tryptophan triad has a favorable redox gradient to translocate one electron from W306 to $FADH^\bullet$ efficiently. Also, assuming the adenine moiety with a similar reduction potential of +1.85 V versus NHE as in the oxidized photolyase,[7,31] the free energy of forward intramolecular ET from the adenine to flavin moieties is about −0.01 eV, and the back ET has a much larger driving force of −1.85 eV. All of the values of reduction potentials are given in Figure 4B and listed in Table S1 (SI), and the resulting free energies are listed in Table S2 (SI). From the derived values, due to the reduction potential change of the cofactor from −0.3 V of FAD to ∼0 V of $FADH^\bullet$, the redox environment at the active site also clearly changes (Figure 4B). The reduction potential of W382, closest to the N5 position of the cofactor $FADH^\bullet$, changes from +1.48 to +1.61 V, a net increase of +130 mV. The reduction potential of the distant W359 has a minor change of +40 mV from +1.41 to +1.45 V. Due to the ultrafast ET of $W382^+$ with W359 and $FADH^-$, we did not detect noticeable ET from W316. Similarly, we also did not observe any ET dynamics from W384 due to the smaller driving force compared with the oxidized state (Figure 4B). Overall, the redox changes at the active site[32] significantly alter the ET dynamics, as shown in Figure 4A for the various ET times, thus leading to the different photoreduction pattern and efficiency.

We can estimate the reorganization energies (λ) for all ET processes from the observed forward and back ET dynamics and further examine their variations of λ due to the environment changes. Assuming all electron tunneling following the superexchange mechanism, we can evaluate the reorganization energies of these ET steps with eq 1[33]

$$\log k_{ET} = 13 - 0.434\beta(r - r_0) - \frac{3.1(\Delta G^0 + \lambda)^2}{\lambda} \quad (1)$$

where k_{ET} is the ET rate in s^{-1}, β here is the empirical electronic coupling parameter in $Å^{-1}$, r is the edge-to-edge separation distance in Å, r_0 is the van der Waals distance at 3.0 Å, ΔG^0 is the total free energy in eV, and λ is the reorganization energy in eV. The β value mostly ranges from 1.0 to 1.4 $Å^{-1}$ in proteins to 1.55−1.65 $Å^{-1}$ in water.[34,35] The distances between ET pairs are shown in Figure 1, and the free energies are derived as above (Table S2, SI). Taking β = 1.4 $Å^{-1}$ as estimated in the oxidized state,[18] we first solved the reorganization energies of 0.24 and 1.16 eV in forward ET and 0.49 and 1.43 eV in back ET for W382/W359 and W359/W306 pairs, respectively. Clearly, the larger reorganization energies of the latter are due to the W306 residue located near the protein surface and exposed to bulk solvent. All of these ET tunneling processes, forward and backward, between different tryptophans are in the Marcus normal region.

We further evaluate the reorganization energies of ET reactions of the isoalloxazine ring with W382 and the adenine

dx.doi.org/10.1021/jz500077s | J. Phys. Chem. Lett. 2014, 5, 820−825

moiety. With β = 1.4 Å^{-1}, the reorganization energies of ET with W382 and the adenine moiety are 1.08 and 0.74 eV for the forward and 1.07 and 1.13 eV for the backward ET, respectively. Figure 4C shows a 2D plot of the Franck−Condon parts of 12 ET steps for the oxidized state and 8 ET steps for the neutral semiquinoid state relative to both the free energy (ΔG^0) and reorganization energy (λ), with an electronic coupling constant of β = 1.4 Å^{-1}. Besides the ET steps for the W359/W306 pair (7−8 and 8−7 in Figure 4C), which has a minor change of their environments and related ET dynamics in the two states, all other ET steps at the active site have obvious variations of both the driving forces (ΔG^0) and reorganization energies (λ), reflecting the changes of the active-site properties in reduction ability and structural flexibility. Referring to the X-ray structures of (6−4) photolyase at the oxidized state[36] and CPD photolyase in the neutral semiquinone state,[17] the N5 atom of the flavin moiety is in close contact (∼3.3 Å) with the carbonyl group of the N378 residue at both the oxidized and neutral semiquinoid states, but for the latter, the position N5 forms a hydrogen bond with the carbonyl group of N378. Also, the N atom of W382 points to the carbonyl group of N378 at a distance of ∼3.6 Å to form a partial hydrogen bond. These new interactions in the neutral semiquinoid state could lead to a local redox change as well as a more rigid and tighter local structure. Such similar changes of hydrogen bond formation have been reported in flavodoxin,[37] and the different active-site relaxation has been observed for the two redox states.[21,38] Thus, from Figure 4C, we observed the obviously different reorganization energies at the active site due to the two different redox states of the cofactor flavin, and thus, the active site in the two states is dynamically different. Finally, all of the analyses of free energies and reorganization energies are based on the equilibrium ET theory. However, all ET steps studied here are nonequilibrium in nature and modulated by the local protein relaxation. A more accurate analysis could be obtained using the Sumi−Marcus 2D model[25] or the recent theoretical method developed by Matyushov.[39]

In this work, we have systematically studied photoreduction of the cofactor flavin in neutral semiquinoid photolyase by integrating femtosecond absorption spectroscopy and site-directed mutagenesis. Comparing with all previous studies, we identified a new intramolecular ET pathway, established the ET dynamics with nonexponential (stretched) behaviors, and refined all of the ET dynamics and time scales for the eight elementary ET reactions. With these ET reaction rates, we further analyzed the ET driving forces and reorganization energies and obtained the reduction potentials of individual ET donors and acceptors, that is, the flavin molecule and the tryptophan triad. Compared with the results from the oxidized photolyase, we observed the significant reduction potential alternation of the active-site W382 residue, and obvious changes of reorganization energies of the ET reactions occurred at the active site. Thus, upon the switch of the reduction state of the cofactor from the oxidized to the semiquinone, the active-site structural and redox properties are changed. Such a change in the active site is correlated, at least, with the local hydrogen bond formation in the semiquinoid state and results in the different photoreduction dynamics that leads to different photoreduction efficiency.

■ ASSOCIATED CONTENT

Supporting Information

The description of experimental methods, systematic data analyses, mutant transients of W382F/W384F, W382F, and W306F (Figures S1−S3), reduction potentials of various species (Table S1), and derived free energies and reorganization energies (Table S2). This material is available free of charge via the Internet at http://pubs.acs.org.

■ AUTHOR INFORMATION

Corresponding Author

*E-mail: zhong.28@asc.ohio-state.edu.

Notes

The authors declare no competing financial interest.

■ ACKNOWLEDGMENTS

We thank Prof. Aziz Sancar for the longtime collaboration on photolyase and Dr. Ya-Ting Kao for the help with the initial experiment. The work was support in part by the National Institute of Health (Grant GM074813), the National Science Foundation (Grant CHE0748358), and the Guggenheim fellowship to D.Z.

■ REFERENCES

(1) Sancar, A. Structure and Function of DNA Photolyase and Cryptochrome Blue-Light Photoreceptors. *Chem. Rev.* **2003**, *103*, 2203−2237.

(2) Kao, Y.-T.; Saxena, C.; Wang, L.; Sancar, A.; Zhong, D. Direct Observation of Thymine Dimer Repair in DNA by Photolyase. *Proc. Nat. Acad. Sci. U.S.A.* **2005**, *102*, 16128−16132.

(3) Liu, Z.; Tan, C.; Guo, X.; Kao, Y.-T.; Li, J.; Wang, L.; Sancar, A.; Zhong, D. Dynamics and Mechanism of Cyclobutane Pyrimidine Dimer Repair by DNA Photolyase. *Proc. Natl. Acad. Sci. U.S.A.* **2011**, *108*, 14831−14836.

(4) Li, J.; Liu, Z.; Tan, C.; Guo, X.; Wang, L.; Sancar, A.; Zhong, D. Dynamics and Mechanism of Repair of Ultraviolet-Induced (6−4) Photoproduct by Photolyase. *Nature* **2010**, *466*, 887−890.

(5) Kavakli, I. H.; Sancar, A. Analysis of the Role of Intraprotein Electron Transfer in Photoreactivation by DNA Photolyase *In Vivo*. *Biochemistry* **2004**, *43*, 15103−15110.

(6) Kim, S. T.; Sancar, A.; Essenmacher, C.; Babcock, G. T. Time-Resolved EPR Studies with DNA Photolyase: Excited-State $FADH^0$ Abstracts an Electron from Trp-306 to Generate $FADH^-$, the Catalytically Active Form of the Cofactor. *Proc. Natl. Acad. Sci. U.S.A.* **1993**, *90*, 8023−8027.

(7) Liu, Z.; Zhang, M.; Guo, X.; Tan, C.; Li, J.; Wang, L.; Sancar, A.; Zhong, D. Dynamic Determination of the Functional State in Photolyase and the Implication for Cryptochrome. *Proc. Natl. Acad. Sci. U.S.A.* **2013**, *110*, 12972−12977.

(8) Heelis, P. F.; Okamura, T.; Sancar, A. Excited-State Properties of *Escherichia coli* DNA Photolyase in the Picosecond to Millisecond Time Scale. *Biochemistry* **1990**, *29*, 5694−5698.

(9) Aubert, C.; Vos, M. H.; Mathis, P.; Eker, A. P. M.; Brettel, K. Intraprotein Radical Transfer during Photoactivation of DNA Photolyase. *Nature* **2000**, *405*, 586−590.

(10) Byrdin, M.; Eker, A. P. M.; Vos, M. H.; Brettel, K. Dissection of the Triple Tryptophan Electron Transfer Chain in *Escherichial coli* DNA Photolyase: Trp382 is the Primary Donor in Photoactivation. *Proc. Nat. Acad. Sci. U.S.A.* **2003**, *100*, 8676−8681.

(11) Lukacs, A.; Eker, A. P.; Byrdin, M.; Villette, S.; Pan, J.; Brettel, K.; Vos, M. H. Role of the Middle Residue in the Triple Tryptophan Electron Transfer Chain of DNA Photolyase: Ultrafast Spectroscopy of a Trp → Phe Mutant. *J. Phys. Chem. B* **2006**, *110*, 15654−15658.

(12) Lukacs, A.; Eker, A. P.; Byrdin, M.; Brettel, K.; Vos, M. H. Electron Hopping through the 15 Å Triple Tryptophan Molecular

Wire in DNA Photolyase Occurs within 30 ps. *J. Am. Chem. Soc.* **2008**, *130*, 14394−14395.
(13) Byrdin, M.; Lukacs, A.; Thiagarajan, V.; Eker, A. P. M.; Brettel, K.; Vos, M. H. Quantum Yield Measurements of Short-Lived Photoactivation Intermediates in DNA Photolyase: Toward a Detailed Understanding of the Triple Tryptophan Electron Transfer Chain. *J. Phys. Chem. A* **2010**, *114*, 3207−3214.
(14) Li, Y. F.; Heelis, P. F.; Sancar, A. Active Site of DNA Photolyase: Tryptophan-306 Is the Intrinsic Hydrogen Atom Donor Essential for Flavin Radical Photoreduction and DNA Repair *In Vitro*. *Biochemistry* **1991**, *30*, 6322−6329.
(15) Saxena, C.; Sancar, A.; Zhong, D. Femtosecond Dynamics of DNA Photolyase: Energy Transfer of Antenna Initiation and Electron Transfer of Cofactor Reduction. *J. Phys. Chem. B* **2004**, *108*, 18026−18033.
(16) Wang, H.; Saxena, C.; Quan, D.; Sancar, A.; Zhong, D. Femtosecond Dynamics of Flavin Cofactor in DNA Photolyase: Radical Reduction, Local Solvation, and Charge Recombination. *J. Phys. Chem. B* **2005**, *109*, 1329−1333.
(17) Park, H. W.; Kim, S. T.; Sancar, A.; Deisenhofer, J. Crystal Structure of DNA Photolyase from *Escherichia coli*. *Science* **1995**, *268*, 1866−1872.
(18) Liu, Z.; Tan, C.; Guo, X.; Li, J.; Wang, L.; Sancar, A.; Zhong, D. Determining Complete Electron Flow in the Cofactor Photoreduction of Oxidized Photolyase. *Proc. Natl. Acad. Sci. U.S.A.* **2013**, *110*, 12966−12971.
(19) Schleicher, E.; Hessling, B.; Illarionova, V.; Bacher, A.; Weber, S.; Richter, G.; Gerwert, K. Light-Induced Reactions of *Escherichia coli* DNA Photolyase Monitored by Fourier Transform Infrared Spectroscopy. *FEBS J.* **2005**, *272*, 1855−1866.
(20) Chang, C.-W.; Guo, L.; Kao, Y.-T.; Li, J.; Tan, C.; Li, T.; Saxena, C.; Liu, Z.; Wang, L.; Sancar, A.; Zhong, D. Ultrafast Solvation Dynamics at Binding and Active Sites of Photolyases. *Proc. Nat. Acad. Sci. U.S.A.* **2010**, *107*, 2914−2919.
(21) Chang, C.-W.; He, T.-F.; Guo, L.; Stevens, J. A.; Li, T.; Wang, L.; Zhong, D. Mapping Solvation Dynamics at the Function Site of Flavodoxin in Three Redox States. *J. Am. Chem. Soc.* **2010**, *132*, 12741−12747.
(22) Kao, Y.-T.; Saxena, C.; He, T.-F.; Guo, L.; Wang, L.; Sancar, A.; Zhong, D. Ultrafast Dynamics of Flavins in Five Redox States. *J. Am. Chem. Soc.* **2008**, *130*, 13132−13139.
(23) Solar, S.; Getoff, N.; Surdhar, P. S.; Armstrong, D. A.; Singh, A. Oxidation of Tryptophan and N-Methylindole by $N_3^{\bullet}$, $Br_2^{\bullet-}$, and $(SCN)_2^{\bullet-}$ Radicals in Light- and Heavy-Water Solutions: a Pulse-Radiolysis Study. *J. Phys. Chem.* **1991**, *95*, 3639−3643.
(24) Candeias, L. P.; Steenken, S. Electron Transfer in Di(deoxy)-nucleoside Phosphates in Aqueous Solution: Rapid Migration of Oxidative Damage (via Adenine) to Guanine. *J. Am. Chem. Soc.* **1993**, *115*, 2437−2440.
(25) Sumi, H.; Marcus, R. A. Dynamic Effects in Electron Transfer Reactions. *J. Chem. Phys.* **1986**, *84*, 4894−4914.
(26) Wang, H. Y.; Lin, S.; Allen, J. P.; Williams, J. C.; Blankert, S.; Laser, C.; Woodbury, N. W. Protein Dynamics Control the Kinetics of Initial Electron Transfer in Photosynthesis. *Science* **2007**, *316*, 747−750.
(27) Liu, Z.; Guo, X.; Tan, C.; Li, J.; Kao, Y.-T.; Wang, L.; Sancar, A.; Zhong, D. Electron Tunneling Pathways and Role of Adenine in Repair of Cyclobutane Pyrimidine Dimer by DNA Photolyase. *J. Am. Chem. Soc.* **2012**, *134*, 8104−8114.
(28) Woiczikowski, P. B.; Steinbrecher, T.; Kubar, T.; Elstner, M. Nonadiabatic QM/MM Simulations of Fast Charge Transfer in *Escherichia coli* DNA Photolyase. *J. Phys. Chem. B* **2011**, *115*, 9846−9863.
(29) Shih, C.; Museth, A. K.; Abrahamsson, M.; Blanco-Rodriguez, A. M.; Di Bilio, A. J.; Sudhamsu, J.; Crane, B. R.; Ronayne, K. L.; Towrie, M.; Vlcek, A., Jr.; et al. Tryptophan-Accelerated Electron Flow through Proteins. *Science* **2008**, *320*, 1760−1762.
(30) Gindt, Y. M.; Schelvis, J. P. M.; Thoren, K. L.; Huang, T. H. Substrate Binding Modulates the Reduction Potential of DNA Photolyase. *J. Am. Chem. Soc.* **2005**, *127*, 10472−10473.
(31) Seidel, C. A. M.; Schulz, A.; Sauer, M. H. M. Nucleobase-Specific Quenching of Fluorescent Dyes. 1. Nucleobase One-Electron Redox Potentials and Their Correlation with Static and Dynamic Quenching Efficiencies. *J. Phys. Chem.* **1996**, *100*, 5541−5553.
(32) Popovic, D. M.; Zmiric, A.; Zaric, S. D.; Knapp, E. W. Energetics of Radical Transfer in DNA Photolyase. *J. Am. Chem. Soc.* **2002**, *124*, 3775−3782.
(33) Page, C. C.; Moser, C. C.; Chen, X. X.; Dutton, P. L. Natural Engineering Principles of Electron Tunnelling in Biological Oxidation−Reduction. *Nature* **1999**, *402*, 47−52.
(34) Gray, H. B.; Winkler, J. R. Electron Transfer in Proteins. *Annu. Rev. Biochem.* **1996**, *65*, 537−561.
(35) Gray, H. B.; Winkler, J. R. Electron Tunneling through Proteins. *Q. Rev. Biophys.* **2003**, *36*, 341−372.
(36) Maul, M. J.; Barends, T. R. M.; Glas, A. F.; Cryle, M. J.; Domratcheva, T.; Schneider, S.; Schlichting, I.; Carell, T. Crystal Structure and Mechanism of a DNA (6−4) Photolyase. *Angew. Chem., Int. Ed.* **2008**, *47*, 10076−10080.
(37) Watt, W.; Tulinsky, A.; Swenson, R. P.; Watenpaugh, K. D. Comparison of the Crystal Structures of a Flavodoxin in Its Three Oxidation States at Cryogenic Temperatures. *J. Mol. Biol.* **1991**, *218*, 195−208.
(38) He, T.-F.; Guo, L.; Guo, X.; Chang, C.-W.; Wang, L.; Zhong, D. Femtosecond Dynamics of Short-Range Protein Electron Transfer in Flavodoxin. *Biochemistry* **2013**, *52*, 9120−9128.
(39) LeBard, D. N.; Kapko, V.; Matyushov, D. V. Energetics and Kinetics of Primary Charge Separation in Bacterial Photosynthesis. *J. Phys. Chem. B* **2008**, *112*, 10322−10342.